Low Part-Per-Trillion, Humidity Resistant Detection of Nitric Oxide Using Microtoroid Optical Resonators

*Yinchao Xu[†§], Allison M. Stanko[†£], Chloe S. Cerione[£], Trevor Lohrey[£], Euan McLeod[§], Brian M. Stoltz[£], and Judith Su[§]**

[†] Y. X. and A. M. S contributed equally

[§]Wyant College of Optical Sciences, The University of Arizona, Tucson, Arizona 85721, United States; Department of Biomedical Engineering, The University of Arizona, Tucson, Arizona 85721, United States

[£] The Warren and Catherine Schlinger Laboratory for Chemistry and Chemical Engineering, Division of Chemistry and Chemical Engineering, California Institute of Technology, Pasadena, California 91125, United States

Keywords: Whispering-gallery mode, microresonator, gas sensor, nitric oxide, RAFT polymerization, ferrocene, humidity resistance

Abstract

The nitric oxide radical plays pivotal roles in physiological as well as atmospheric contexts. Although the detection of dissolved nitric oxide *in vivo* has been widely explored, highly sensitive (i.e. low part-per-trillion level), selective, and humidity resistant detection of gaseous nitric oxide in air remains challenging. In the field, humidity can have dramatic effects on the accuracy and selectivity of gas sensors, confounding data and leading to overestimation of gas concentration. Highly selective and humidity resistant gaseous NO sensors based on laser-induced graphene (LIG) were recently reported, displaying a limit of detection (LOD) of 8.3 ppb. Although highly sensitive (LOD = 590 ppq) single-wall carbon nanotube NO sensors have been reported, these sensors lack selectivity and humidity resistance. In this report, we disclose a highly sensitive (LOD = 2.34 ppt), selective, and humidity resistant nitric oxide sensor based on a whispering-gallery mode (WGM) microtoroid optical resonator. Excellent analyte selectivity was enabled via novel ferrocene-containing polymeric coatings synthesized via RAFT polymerization. Utilizing a Frequency Locked Optical Whispering Evanescent Resonator (FLOWER) system, the microtoroid's real-time resonance frequency shift response to nitric oxide, was tracked with sub-femtometer resolution. The lowest concentration experimentally detected was 6.4 ppt, which is the lowest reported to date. Additionally, the performance of the sensor remained consistent across different humidity environments. Lastly, the impact of the chemical composition and molecular weight of the novel ferrocene-containing polymeric coatings on sensing performance was evaluated. We anticipate that our results will have impact on a wide variety of fields where NO sensing is important such as medical diagnostics through exhaled breath, determination of planetary habitability, marine science, climate change, air quality monitoring, and treating cardiovascular and neurological disorders.

Introduction

Systems for the selective and rapid detection of gases are important tools used to monitor environmental impacts,[1] occupational safety,[2] and human biomarkers.[3] Nitric oxide is a common byproduct of vehicle exhaust and industrial processes involving combustion, making it a main contributor to air pollution.[4] In fact, nitric oxide is a major industrial emission contributing to ozone layer depletion.[5] In addition to its environmental impacts, nitric oxide also serves as an important biomarker of respiratory health. Higher concentrations of exhaled nitric oxide are associated with asthma and Chronic Obstructive Pulmonary Disease (COPD), and the exhaled nitric oxide (F_ENO) test is commonly administered in the diagnosis of these diseases.[6] Furthermore, nitric oxide is easily oxidized in air to nitrogen dioxide, a common air pollutant which is highly corrosive and toxic and has been implicated as a danger to human respiratory health.[7] To mitigate injury due to gas exposure and monitor the environmental impacts of industrial processes, selective sensors for NO detection must be developed and deployed.[8] Additionally, for sensors to produce reliable and reproducible results in the field, resistance to external environmental factors such as humidity must be demonstrated.

A variety of sensors have been established for nitric oxide monitoring, including chemical electrode sensors,[9] chemiresistive gas sensors (CGS),[10–14] Rayleigh surface acoustic wave resonators (RSAW)[15,16], and chemiluminescence-based sensors.[17] The lowest limits of NO detection (sub-ppt) have been achieved with single-wall carbon nanotube (SWNT) based sensors, albeit with a lack of analyte specificity and lab-to-lab perturbations in sensitivity.[11] Semiconductor metal oxide based chemiresistive gas sensors have also demonstrated merit in NO sensing, however their practicality is limited by their extreme operating temperatures.[18] Additionally, chemiresistive gas sensors often display poor humidity tolerance due to the competitive absorption of water onto metal oxide semiconductor surfaces.[19] Recently, the development of humidity

resistant materials for gas sensing has received much attention.[20–22] Highly practical, wearable, flexible, and humidity resistant NO/NO_2 gas sensors based on laser-induced graphene were recently reported by Yang and coworkers, displaying a LOD of 8.3 ppb for NO.[10] Despite this advance, there have been no reports of part-per-trillion level nitric oxide sensors that are selective as well as humidity resistant, a gap which we aimed to address through our research efforts.

Recently, our lab developed a platform for selective, ultra-sensitive gas sensing using whispering-gallery mode (WGM) microtoroid sensors coated with polymer brushes.[23] WGM optical microresonators have attracted intense interest in the past decades due to their high quality factors (Q) and small mode volumes, which cause enhanced light matter interaction. In WGM microresonators, photons will take hundreds of thousands of round trips while interacting with analytes on the surface, significantly increasing the optical sensing signal response to analytes. Since 2002, sensing based on WGM mode shift has developed a wide application area, including proteins,[24–27] gases,[23] exosomes,[28,29] nanoparticles,[24] viruses,[30] and even single molecules.[24,31] Frequency locked optical whispering evanescent resonator (FLOWER) is a sensing system that provides a lock-in method to track WGM resonances in real time with high (sub-femtometer) resolution.[24,27,32–35] This system allows us to further investigate the resonance shift of a WGM sensor at timescales as short as milliseconds when the sensor is placed in a continuously changing external environment. FLOWER provides advantages over plasmonic[36] or hybrid plasmonic-WGM sensors[37] in that it uses a bare microcavity, which enables a greater capture area and thus response time.[38]

In this research, we create a WGM gas-sensing platform to enable selective nitric oxide sensing in the low part-per-trillion range (6.4 ppt – 240 ppt). This is two orders of magnitude lower than what has previously been demonstrated with whispering gallery mode sensors for volatile

organics such as DIMP, ammonia, and formaldehyde.[39] Co-polymers of 2-(methacryloyloxy) ferrocenecarboxylate (FcMA) and methyl methacrylate (MMA) were synthesized and deposited on the surface of the microtoroid in a polymer brush. We hypothesized that the binding of nitric oxide to the iron centers in the polymer would lead to swelling of the coating and a change in refractive index, causing a WGM resonance shift. While polymers of this type have been previously accessed via free-radical polymerization[40] and atom-transfer radical polymerization,[41] to the best of our knowledge, this is the first report of FcMA/MMA statistical co-polymers prepared via reversible addition fragmentation chain-transfer (RAFT) polymerization. Employing RAFT polymerization allowed us to access polymers with precise control over molecular weight while ensuring end-group fidelity. By testing polymeric coatings with various molecular weights and ferrocene content in our gas sensing experiments, we gauged the impacts of these factors on sensor performance. Additionally, our sensor displayed excellent specificity for NO, exhibiting no response greater than blank noise to volatile organics including benzene, hexanes, and diisopropyl methylphosphonate (DIMP). To evaluate the selectivity and practicality of our device, we tested it in different humidity environments, finding that sensor's response was consistent despite changes in humidity.

Experimental Methods

a) Polymer Synthesis and Microtoroid Coating

Statistical co-polymers of 2-(methacryloyloxy) ferrocenecarboxylate and methyl methacrylate were prepared via RAFT polymerization (Scheme 1). Chain transfer agent CTA-OSu and radical initiator Int-OSu were employed to reliably install the desired succinimide ester end group needed for toroid functionalization. Polymer A was prepared by employing a 1: 10 ratio of

FcMA to MMA, leading to a statistical co-polymer with a 1: 8.8 ratio of FcMA: MMA units (determined by ^{1}H NMR) and a M_n of 10.1 kDa, with excellent polydispersity of M_n/M_w = 1.032. Polymer B was prepared in the same fashion, however a 1: 20 ratio of FcMA to MMA was employed, leading to a polymer with M_n ~ 8.5 kDa, M_n/M_w ~ 1.08 and a FcMA: MMA ratio of 1: 18.5.

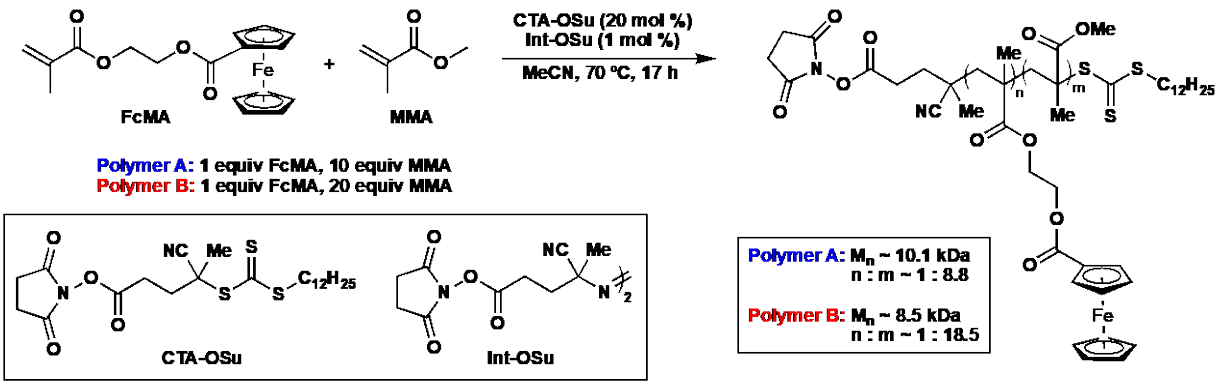

Scheme 1. Synthesis of statistical copolymers of 2-(methacryloyloxy) ferrocenecarboxylate and methyl methacrylate via RAFT polymerization.

Microdisks were fabricated as previously described[24] in a cleanroom via photolithography, patterning, and etching. Then, the silica microdisk was reflowed using a carbon dioxide laser to form a microtoroid structure with a major radius of 100 μm in diameter and a minor radius of 10 μm. Following plasma treatment of the microtoroid surface, the chip was immersed in a glass vial containing a 1% solution of 3-(aminopropyl) triethoxysilane (APTES) in 990 µL of chloroform, functionalizing the silica surface with free amine groups (Scheme 2). The vial was placed on a nutator for 10 min and the chip was then rinsed with chloroform and dried with nitrogen. Afterwards, the chip was immersed in a 5 mM solution of either Polymer A or Polymer B for 2 hours, depositing the polymer brush via an on-toroid amide coupling reaction. The chip was rinsed and blown-dry and then baked on a 100 ˚C hotplate for 30 min to evaporate most of the solvent

and enhance the stability of the surface. Lastly, the chip was placed in a room-temperature vacuum overnight to thoroughly remove residual solvent.

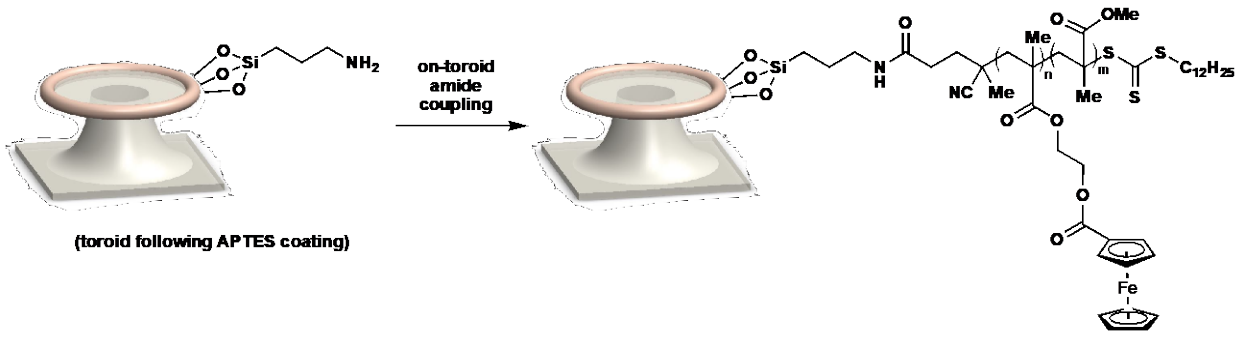

Scheme 2. Deposition of polymer brush onto microtoroid surface.

Gas Sensing

The chip was placed inside a small chamber (Figure 1a) enclosed inside a larger 20 cm × 10 cm × 10 cm stainless steel box connected to a vacuum to remove residual gas. A TEC element (Thorlabs TECD2S) was placed at the bottom of the small chamber. The small chamber was designed to reduce the space for diffusion and to make gas flow reach the microtoroid more evenly. A FlexStream™ Gas Standard Generator was connected to a flowmeter to read the exact flow rate into the chamber and then connected to the chamber to blow a target gas at a specific flow rate and concentration. The target gas was generated by mixing high concentration gas from a permeation tube and a gas carrier (either nitrogen or argon). This brings the gas to a secondary dilution system for further dilution to low part-per-trillion values. The concentration was controlled by adjusting the primary dilution flow rate ,F_{pd}, the component gas flow rate, F_c, and diluted gas rate, F_{sd}, in the second dilution system. The final diluted gas concentration in ppm unit C_{ppmv} is given by:

$$C_{ppmv} = \frac{E_{ng/min} \times 22.41\ \mathrm{L/mol}}{MW \times F_{pd}} \times \frac{F_c}{F_c + F_{sd}} \quad (1)$$

where MW is molecule weight of target gas and $E_{ng/min}$ is the emission rate of the permeation tube. The flowmeter sets the flow rate after the second dilution system.

The FLOWER system uses a tunable laser (Velocity TLB-6700).The laser light polarization is adjusted by a polarization controller and goes through a 50:50 fiber splitter. One beam goes directly to a balanced photodetector (PD) while another goes through a tapered optical fiber. The balanced PD minimizes the effects of laser power fluctuations. A 24-bit data acquisition (DAQ) card collects the real time wavelength signal from both the laser and the temperature sensor. The fundamental mode was selected for tracking, as it exhibits the highest quality factors and greatest field area overlap with the polymer layer where the gas absorption is changing the optical properties of the layer (Figure 1c). Afterwards, the laser wavelength was locked-in to the selected fundamental mode and the DAQ monitored both the laser wavelength shift and the temperature sensor to give the raw data of WGM resonance and temperature.

Before testing the response to nitric oxide, argon was blown into the sample chamber for 30 minutes until thermal equilibration occurred. During an experiment, we cycled between blowing in pure argon for 10 minutes as a blank comparison and blowing in the mixed target gas and gas carrier for another 10 minutes. Argon was chosen as the carrier gas for the nitric oxide sensing experiments, as it is more dense than nitric oxide and therefore can reliably displace it in between cycles. After completing one cycle, recording was stopped for several minutes until the residual waste gas was removed and the chamber re-filled with pure argon (Figure 2).

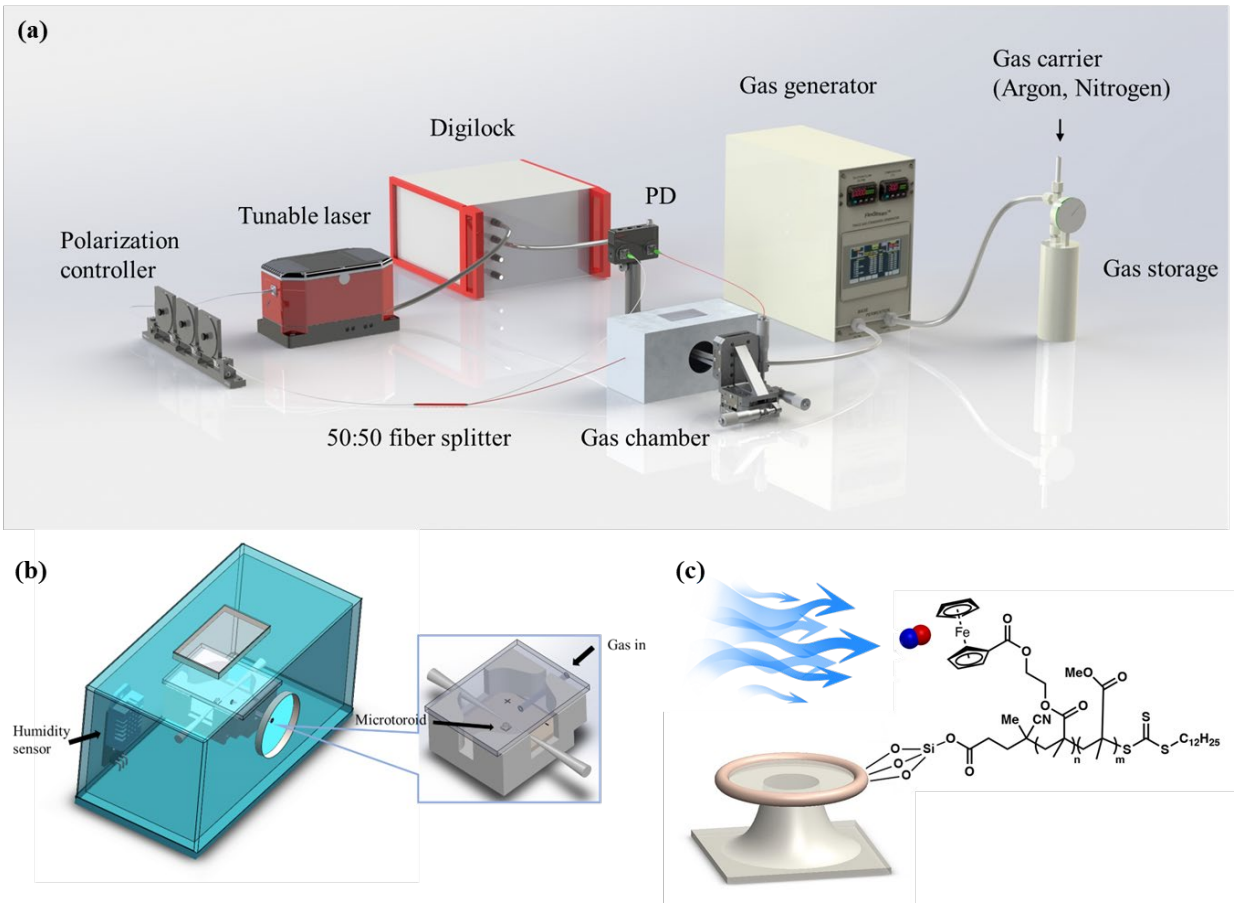

Figure 1 (a) Nitric oxide gas sensing schematic. FLOWER consists of a tunable laser (Velocity TLB-6700), Digilock frequency locking feedback controller, polarization controller, fiber splitter, balanced photodetector (PD) and microtoroid. (b) Gas chamber with humidity sensor and coupled toroid. Inset. Schematic of an optical fiber coupled to a microtoroid. The small chamber is designed with a slit for the gas delivery tube. A TEC (thermoelectic cooler) is set at the bottom of the chamber. A temperature sensor is placed between the toroid and the inlet gas tube (not shown in the figure). A glass top is used to keep the gas flow stable and directed to the other side of chamber. (c) Schematic of the coated microtoroid and nitric oxide binding process.

Results and Discussion

The WGM resonance wavelength (**Δλ**) was measured in real time at concentrations from 6.4 ppt to 240 ppt (Figure 2). The chamber was purged with argon between each concentration tested in order to release any NO absorbed in the polymer coating. Linear fits were assigned to track the sensor's response during the intervals of Ar purging (white intervals) and nitric oxide exposure (red intervals).

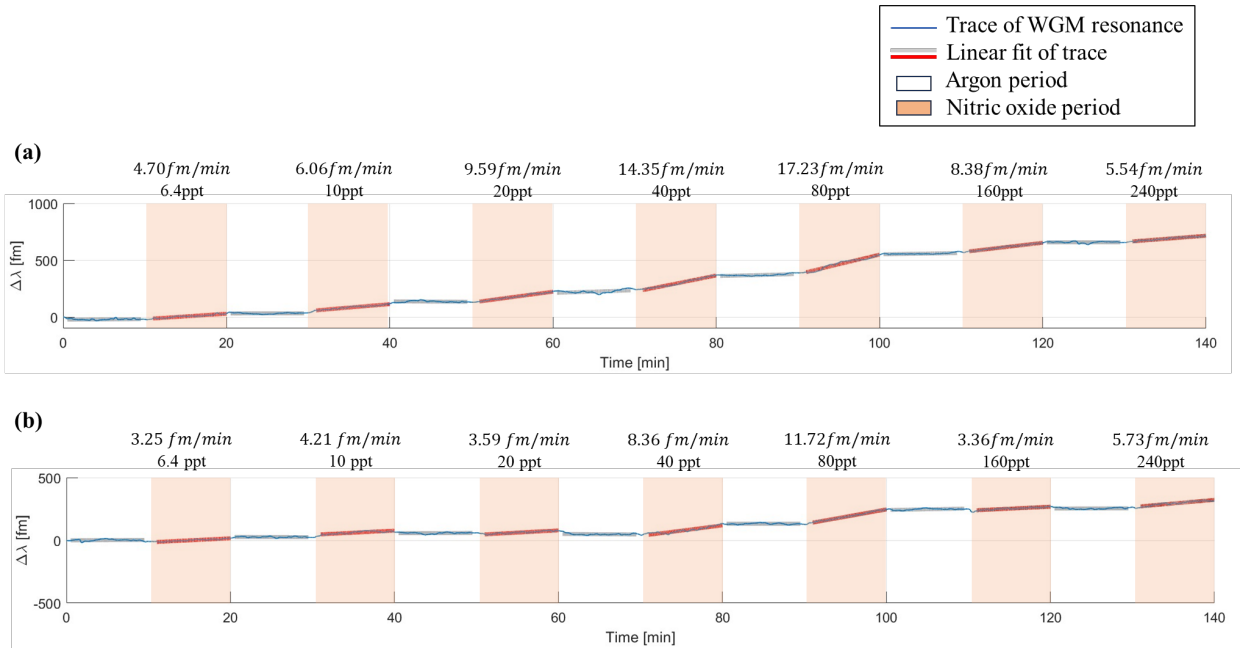

Figure 2 (a) FLOWER response to nitric oxide using a Polymer A as the toroid coating. (b) FLOWER response to nitric oxide sensing using Polymer B as the toroid coating.

Nitric oxide detection real-time traces post temperature calibration are shown in Figure 3, where the sensor's response is plotted against nitric oxide concentration. The wavelength shift value (**Δλ**) is the relative wavelength shift from the starting point. The slope of the wavelength shift over time is considered to be the target gas response. Langmuir's theory of adsorption[42] is applied in our case to describe the molecule binding dynamic and fit the curve of response. The two groups of data were fit to:

$$y = \frac{Bx}{\kappa_d + x} \quad (2)$$

where B and κ_d are both fitting parameters (Figure 3b). By calculating the intersection point between the curve and the blank signal (1.5 fm/min), we derived the LOD (limit of detection) of the sensor for Polymer A to be 2.43 ppt and Polymer B to be 2.91 ppt. The response slope was relatively consistent across trials for concentrations from 0 to 100 ppt. However, it was noted that the sensor's response began to decrease when concentrations above 100 ppt were tested, implying that the polymer coating on the toroid was quickly saturating with gas. Concentrations above 240 ppt could also be detected, although this causes the sensor to saturate (Figure S5, Supporting Information). This capability can be valuable for issuing early warnings, as it allows for the detection of NO concentrations within the 6.4 to 240 ppt range, while also indicating when larger concentrations are present. The sensor can also be recovered using heat, thus making it reusable after saturation (Figure S2, Supporting Information).

The impact of the chemical composition and molecular weight of the polymeric coating on the toroid was also evaluated. Polymer A, which contains a higher ratio of FcMA to MMA, displayed a higher response slope than Polymer B for concentrations between 0 and 100 ppt. Polymer A contains twice as many Fe binding sites for nitric oxide relative to Polymer B, thereby increasing the swelling of the polymer coating and producing a higher response slope. Polymer coatings of lower (~ 6.9 kDa) and higher (~ 19.2 kDa) molecular weights were also tested, but these either provided lower response slopes or saturated more quickly (Figure S4, Supporting Information). Additionally, a polymer coating with low molecular weight (~ 5.0 kDa) but high FcMA content (1 : 5.7 ratio of FcMA:MMA) produced an irreversible response to NO at ppb-level concentrations (Figure S5b, Supporting Information).

To test the practicality of our sensor in the field, we also measured its response to NO in different humidity environments (Figure 3c). Due to the hydrophobic nature of the polymer coating, we anticipated the sensor's performance would remain consistent.[43] Indeed, the sensor displayed a similar response at 47% humidity as compared to 20% humidity. Notably, this is the first report of a humidity resistant, part-per-trillion level nitric oxide sensor.

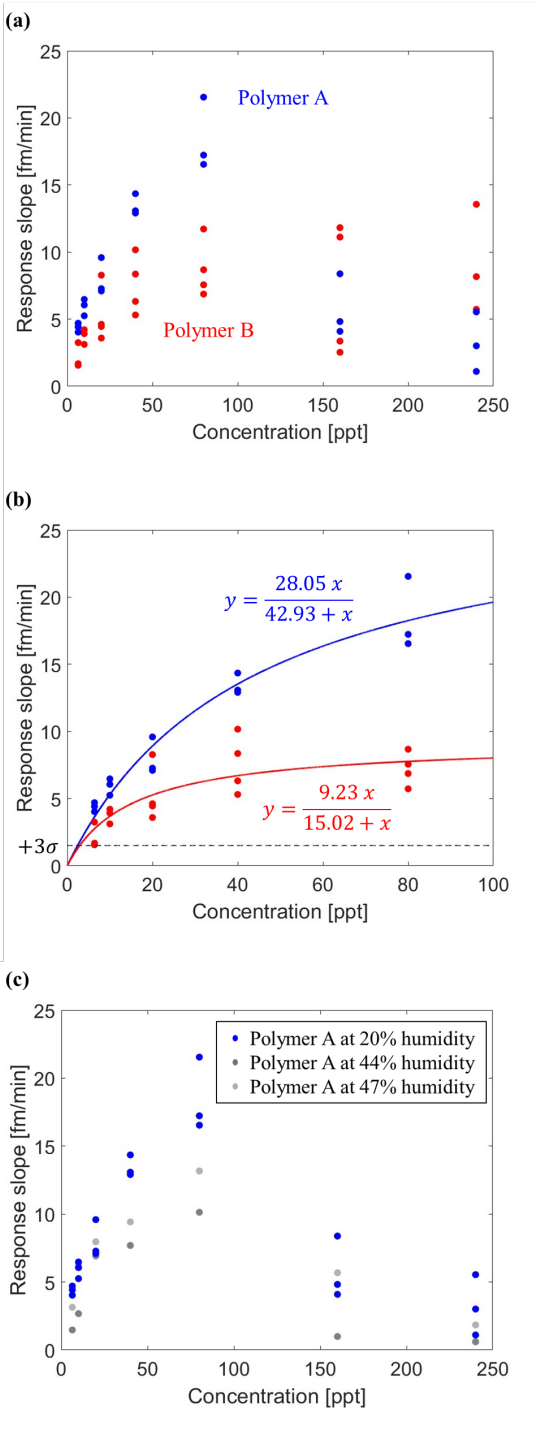

Figure 3 (a) Plot of the sensor response to the tested concentrations of nitric oxide. (b) One-site specific binding curve fit of each response trace. The blank signal is represented by a dashed line. (c) Sensor coated with polymer A response to nitric oxide in different humidity environments.

In addition to humidity resistance, the sensor reported herein also demonstrates excellent selectivity for nitric oxide when compared to other hazard gases including diisopropyl methylphosphonate (DIMP), hexane, and benzene. (Figure 4a-c) None of these gases gave a response higher than the blank signal, even when tested at part-per-billion level concentrations.

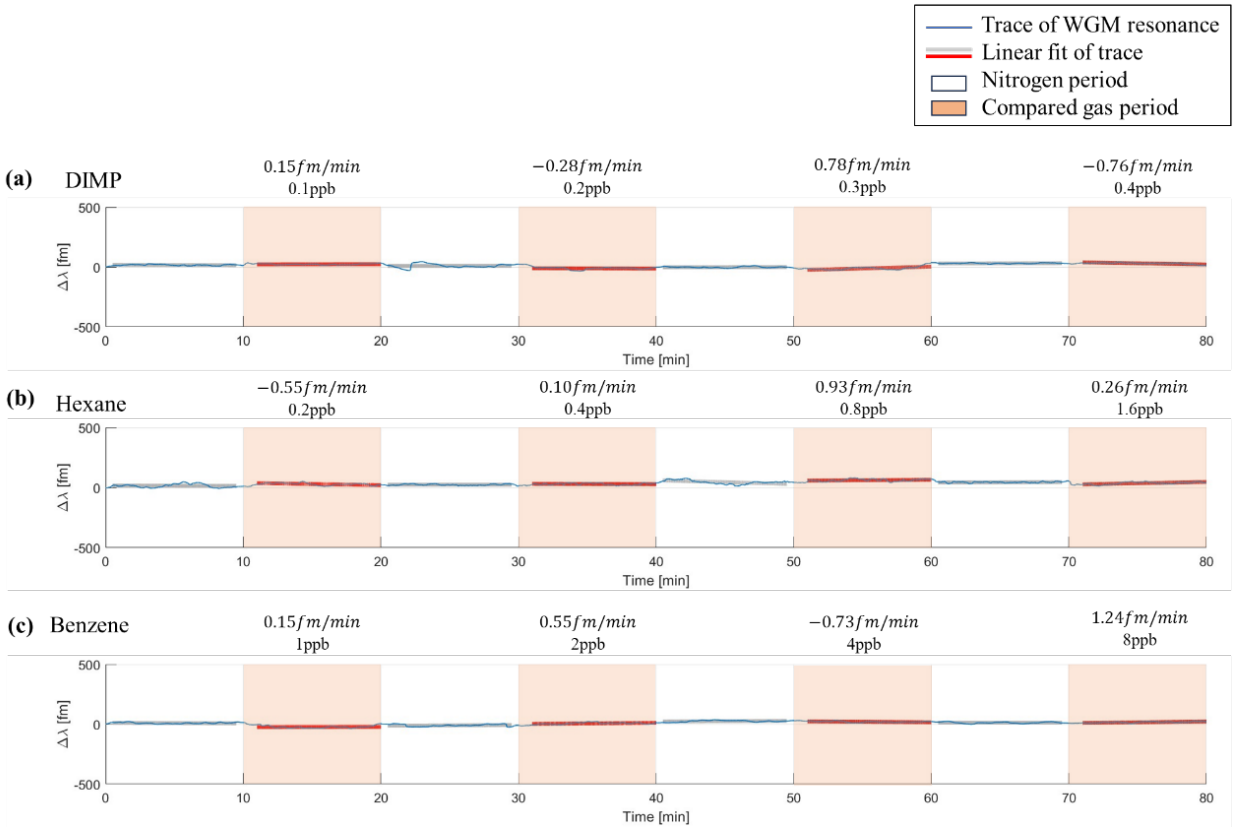

Figure 4 Selectivity demonstration of the FLOWER nitric oxide sensor. The sensor is tested in response to (a) DIMP, (b) hexane, (c) benzene. The grey and red line are linear fits to the blank (nitrogen) and the target gas response.

In comparison to existing technologies for nitric oxide sensing, the FLOWER sensor reported herein displayed the lowest experimentally detected concentration to date of 6.4 ppt, with an LOD of 2.43 ppt (Table 1). Slightly lower limits of detection were reported for carbon nanotube sensors[11], albeit with a lack of selectivity. Except for carbon nanotube sensors, our FLOWER

sensor is the only other reported device that can measure nitric oxide in the low part-per-trillion range, and its humidity resistance and selectivity provide distinct advantages over existing nitric oxide sensors.

Table 1. Comparison of FLOWER-based NO sensor against existing technologies.

Sensing Technique	Calculated LOD	Concentration Range	Lowest Concentration Experimentally Detected	References
FLOWER	2.43 ppt	6.4 ppt – 240 ppt	6.4 ppt	This paper
Carbon nanotube chemiresistor	590 ppq	10 ppt – 500ppm	10 ppt	[11]
Carbon nanotube chemiresistor	0.2 ppb	100 ppb – 5 ppm	100 ppb	[12]
Graphene chemiresistor		2 ppb – 420 ppb	2 ppb	[13]
LIG chemiresistor	8.3 ppb	20 ppb – 1 ppm	20 ppb	[10]
ZnO chemiresistor	10 ppb	10 ppb – 1 ppm	10 ppb	
Nanowire chemiresistor	10 ppb	0.5 ppm – 200ppm	0.5 ppm	[14]
RSAW resonator	23 ppb	100 ppb –700ppb	100 ppb	[15]
RSAW resonator		1 ppb – 200 ppb	1 ppb	[16]
Chemical electrode	350 ppb	2.5 ppm – 10 ppm	2.5 ppm	[9]

Conclusions

In this paper, we exhibit low part-per-trillion level selective nitric oxide detection using WGM microtoroids functionalized with novel polymeric coatings. We synthesized ferrocene-containing polymers via RAFT polymerization that enable the sensor's selective responsive to nitric oxide, finding that more ferrocene-rich polymers with molecular weights around 10 kDa displayed the best sensing capabilities. With FLOWER real-time resonance tracking, we experimentally detected nitric oxide in concentrations as low as 6.4 ppt, the lowest experimentally demonstrated concentration reported in the literature, and we theoretically calculated an LOD of 2.43 ppt with a one-site binding model. Humidity resistance of the sensor was enabled by the hydrophobic nature of the polymer coatings employed. Control experiments with several hazardous gases demonstrated the selectivity of our sensor to nitric oxide.

Supporting Information. The supporting information is available free of charge at (insert link here)

Polymer synthesis and characterization, synthetic protocols, NMR spectra, size exclusion chromatography data, sensor response to polymers with M_n ~ 6.9 kDa and M_n ~ 19.4 kDa, sensor response to ferrocene monolayer

AUTHOR INFORMATION

Corresponding Author

*judy@optics.arizona.edu

Author Contributions

Y.X. performed gas-sensing experiments and data analysis. A.M.S., C.S.C., and T.L. designed, synthesized, and characterized polymers. E.M. was involved in the sensing part of the project design. B.M.S. directed and guided the chemical synthesis. J.S. conceived the idea for the project and guided the overall project. A.M.S., Y.X., and J.S. wrote the manuscript.

Funding Sources

This work was funded by the Defense Threat Reduction Agency (HDTRA1-18-1-0044).

ABBREVIATIONS

WGM, whispering gallery mode, RAFT, reversible addition-fragmentation chain-transfer, FLOWER, frequency locked optical whispering evanescent resonator, FcMA, 2-(methacryloyloxy) ferrocenecarboxylate, MMA, methyl methacrylate LOD, limit of detection, DIMP, diisopropyl methylphosphonate

REFERENCES

(1) Dhall, S.; Mehta, B. R.; Tyagi, A. K.; Sood, K. A Review on Environmental Gas Sensors: Materials and Technologies. *Sensors International* **2021**, *2*, 100116. https://doi.org/10.1016/j.sintl.2021.100116.

(2) Bag, A.; Lee, N.-E. Recent Advancements in Development of Wearable Gas Sensors. *Advanced Materials Technologies* **2021**, *6* (3), 2000883. https://doi.org/10.1002/admt.202000883.

(3) Privett, B. J.; Shin, J. H.; Schoenfisch, M. H. Electrochemical Nitric Oxide Sensors for Physiological Measurements. *Chem. Soc. Rev.* **2010**, *39* (6), 1925–1935. https://doi.org/10.1039/B701906H.

(4) Kampa, M.; Castanas, E. Human Health Effects of Air Pollution. *Environmental Pollution* **2008**, *151* (2), 362–367. https://doi.org/10.1016/j.envpol.2007.06.012.

(5) Ravishankara, A. R.; Daniel, J. S.; Portmann, R. W. Nitrous Oxide (N2O): The Dominant Ozone-Depleting Substance Emitted in the 21st Century. *Science* **2009**, *326* (5949), 123–125. https://doi.org/10.1126/science.1176985.

(6) Taylor, D. R.; Pijnenburg, M. W.; Smith, A. D. Exhaled Nitric Oxide Measurements: Clinical Application and Interpretation. *Thorax* **2006**, *61* (9), 817–827. https://doi.org/10.1136/thx.2005.056093.

(7) Faustini, A.; Rapp, R.; Forastiere, F. Nitrogen Dioxide and Mortality: Review and Meta-Analysis of Long-Term Studies. *European Respiratory Journal* **2014**, *44* (3), 744–753. https://doi.org/10.1183/09031936.00114713.

(8) Ménil, F.; Coillard, V.; Lucat, C. Critical Review of Nitrogen Monoxide Sensors for Exhaust Gases of Lean Burn Engines. *Sensors and Actuators B: Chemical* **2000**, *67* (1), 1–23. https://doi.org/10.1016/S0925-4005(00)00401-9.

(9) Lin, C.-Y.; Chen, J.-G.; Hu, C.-W.; Tunney, J. J.; Ho, K.-C. Using a PEDOT:PSS Modified Electrode for Detecting Nitric Oxide Gas. *Sensors and Actuators B: Chemical* **2009**, *140* (2), 402–406. https://doi.org/10.1016/j.snb.2009.04.041.

(10) Yang, L.; Zheng, G.; Cao, Y.; Meng, C.; Li, Y.; Ji, H.; Chen, X.; Niu, G.; Yan, J.; Xue, Y.; Cheng, H. Moisture-Resistant, Stretchable NOx Gas Sensors Based on Laser-Induced Graphene for Environmental Monitoring and Breath Analysis. *Microsyst Nanoeng* **2022**, *8* (1), 1–12. https://doi.org/10.1038/s41378-022-00414-x.

(11) Chen, G.; Paronyan, T. M.; Pigos, E. M.; Harutyunyan, A. R. Enhanced Gas Sensing in Pristine Carbon Nanotubes under Continuous Ultraviolet Light Illumination. *Sci Rep* **2012**, *2* (1), 343. https://doi.org/10.1038/srep00343.
(12) Jeon, J.-Y.; Kang, B.-C.; Byun, Y. T.; Ha, T.-J. High-Performance Gas Sensors Based on Single-Wall Carbon Nanotube Random Networks for the Detection of Nitric Oxide down to the Ppb-Level. *Nanoscale* **2019**, *11* (4), 1587–1594. https://doi.org/10.1039/C8NR07393G.
(13) Li, W.; Geng, X.; Guo, Y.; Rong, J.; Gong, Y.; Wu, L.; Zhang, X.; Li, P.; Xu, J.; Cheng, G.; Sun, M.; Liu, L. Reduced Graphene Oxide Electrically Contacted Graphene Sensor for Highly Sensitive Nitric Oxide Detection. *ACS Nano* **2011**, *5* (9), 6955–6961. https://doi.org/10.1021/nn201433r.
(14) Singh, P.; Hu, L.-L.; Zan, H.-W.; Tseng, T.-Y. Highly Sensitive Nitric Oxide Gas Sensor Based on ZnO-Nanorods Vertical Resistor Operated at Room Temperature. *Nanotechnology* **2019**, *30* (9), 095501. https://doi.org/10.1088/1361-6528/aaf7cb.
(15) Wang, S.-H.; Kuo, S.-H.; Shen, C.-Y. A Nitric Oxide Gas Sensor Based on Rayleigh Surface Acoustic Wave Resonator for Room Temperature Operation. *Sensors and Actuators B: Chemical* **2011**, *156* (2), 668–672. https://doi.org/10.1016/j.snb.2011.02.016.
(16) Wang, S.-H.; Shen, C.-Y.; Su, J.-M.; Chang, S.-W. A Room Temperature Nitric Oxide Gas Sensor Based on a Copper-Ion-Doped Polyaniline/Tungsten Oxide Nanocomposite. *Sensors* **2015**, *15* (4), 7084–7095. https://doi.org/10.3390/s150407084.
(17) Robinson, J. K.; Bollinger, M. J.; Birks, J. W. Luminol/H2O2 Chemiluminescence Detector for the Analysis of Nitric Oxide in Exhaled Breath. *Anal. Chem.* **1999**, *71* (22), 5131–5136. https://doi.org/10.1021/ac990646d.
(18) Sun, Y.-F.; Liu, S.-B.; Meng, F.-L.; Liu, J.-Y.; Jin, Z.; Kong, L.-T.; Liu, J.-H. Metal Oxide Nanostructures and Their Gas Sensing Properties: A Review. *Sensors* **2012**, *12* (3), 2610–2631. https://doi.org/10.3390/s120302610.
(19) Wang, Y.; Zhou, Y. Recent Progress on Anti-Humidity Strategies of Chemiresistive Gas Sensors. *Materials (Basel)* **2022**, *15* (24), 8728. https://doi.org/10.3390/ma15248728.
(20) Song, Z.; Huang, Z.; Liu, J.; Hu, Z.; Zhang, J.; Zhang, G.; Yi, F.; Jiang, S.; Lian, J.; Yan, J.; Zang, J.; Liu, H. Fully Stretchable and Humidity-Resistant Quantum Dot Gas Sensors. *ACS Sens.* **2018**, *3* (5), 1048–1055. https://doi.org/10.1021/acssensors.8b00263.
(21) Wang, J.; Yang, P.; Wei, X. High-Performance, Room-Temperature, and No-Humidity-Impact Ammonia Sensor Based on Heterogeneous Nickel Oxide and Zinc Oxide Nanocrystals. *ACS Appl. Mater. Interfaces* **2015**, *7* (6), 3816–3824. https://doi.org/10.1021/am508807a.
(22) Yoon, J.-W.; Kim, J.-S.; Kim, T.-H.; Hong, Y. J.; Kang, Y. C.; Lee, J.-H. A New Strategy for Humidity Independent Oxide Chemiresistors: Dynamic Self-Refreshing of In2O3 Sensing Surface Assisted by Layer-by-Layer Coated CeO2 Nanoclusters. *Small* **2016**, *12* (31), 4229–4240. https://doi.org/10.1002/smll.201601507.
(23) Li, C.; Lohrey, T.; Nguyen, P.-D.; Min, Z.; Tang, Y.; Ge, C.; Sercel, Z.; McLeod, E.; Stoltz, B.; Su, J. Part-per-Trillion Trace Selective Gas Detection Using Frequency Locked Whispering Gallery Mode Microtoroids. **2022**. https://doi.org/10.26434/chemrxiv-2022-606xv.
(24) Su, J.; Goldberg, A. F.; Stoltz, B. M. Label-Free Detection of Single Nanoparticles and Biological Molecules Using Microtoroid Optical Resonators. *Light Sci Appl* **2016**, *5* (1), e16001–e16001. https://doi.org/10.1038/lsa.2016.1.

(25) Luu, G. T.; Ge, C.; Tang, Y.; Li, K.; Cologna, S. M.; Godwin, A. K.; Burdette, J. E.; Su, J.; Sanchez, L. M. An Integrated Approach to Protein Discovery and Detection from Complex Biofluids. *Molecular & Cellular Proteomics* **2023**, *0* (0). https://doi.org/10.1016/j.mcpro.2023.100590.
(26) Lu, T.; Su, T.-T. J.; Vahala, K. J.; Fraser, S. E. Split Frequency Sensing Methods and Systems. US8593638B2, November 26, 2013. https://patents.google.com/patent/US8593638B2/en (accessed 2022-10-13).
(27) Ozgur, E.; Roberts, K. E.; Ozgur, E. O.; Gin, A. N.; Bankhead, J. R.; Wang, Z.; Su, J. Ultrasensitive Detection of Human Chorionic Gonadotropin Using Frequency Locked Microtoroid Optical Resonators. *Anal. Chem.* **2019**, *91* (18), 11872–11878. https://doi.org/10.1021/acs.analchem.9b02630.
(28) Su, J. Label-Free Single Exosome Detection Using Frequency-Locked Microtoroid Optical Resonators. *ACS Photonics* **2015**, *2* (9), 1241–1245. https://doi.org/10.1021/acsphotonics.5b00142.
(29) Su, J. Label-Free Biological and Chemical Sensing Using Whispering Gallery Mode Optical Resonators: Past, Present, and Future. *Sensors* **2017**, *17* (3), 540. https://doi.org/10.3390/s17030540.
(30) Shao, L.; Jiang, X.-F.; Yu, X.-C.; Li, B.-B.; Clements, W. R.; Vollmer, F.; Wang, W.; Xiao, Y.-F.; Gong, Q. Detection of Single Nanoparticles and Lentiviruses Using Microcavity Resonance Broadening. *Advanced Materials* **2013**, *25* (39), 5616–5620. https://doi.org/10.1002/adma201302572.
(31) Yu, X.-C.; Tang, S.-J.; Liu, W.; Xu, Y.; Gong, Q.; Chen, Y.-L.; Xiao, Y.-F. Single-Molecule Optofluidic Microsensor with Interface Whispering Gallery Modes. *Proceedings of the National Academy of Sciences* **2022**, *119* (6), e2108678119. https://doi.org/10.1073/pnas.2108678119.
(32) AU - Su, J. Label-Free Single Molecule Detection Using Microtoroid Optical Resonators. *JoVE* **2015**, No. 106, e53180. https://doi.org/10.3791/53180.
(33) Hao, S.; Su, J. Noise-Induced Limits of Detection in Frequency Locked Optical Microcavities. *Journal of Lightwave Technology* **2020**, *38* (22), 6393–6401. https://doi.org/10.1109/JLT.2020.3010869.
(34) Hao, S.; Suebka, S.; Su, J. Single 5-Nm Quantum Dot Detection via Microtoroid Optical Resonator Photothermal Microscopy. arXiv September 14, 2023. https://doi.org/10.48550/arXiv.2309.07898.
(35) Luu, G. T.; Ge, C.; Tang, Y.; Li, K.; Cologna, S. M.; Godwin, A. K.; Burdette, J. E.; Su, J.; Sanchez, L. M. An Integrated Approach to Protein Discovery and Detection From Complex Biofluids. *Molecular & Cellular Proteomics* **2023**, *22* (7). https://doi.org/10.1016/j.mcpro.2023.100590.
(36) Nguyen, P.-D.; Zhang, X.; Su, J. One-Step Controlled Synthesis of Size-Tunable Toroidal Gold Particles for Biochemical Sensing. *ACS Appl. Nano Mater.* **2019**, *2* (12), 7839–7847. https://doi.org/10.1021/acsanm.9b01856.
(37) Li, C.; Chen, L.; McLeod, E.; Su, J. Dark Mode Plasmonic Optical Microcavity Biochemical Sensor. *Photon. Res., PRJ* **2019**, *7* (8), 939–947. https://doi.org/10.1364/PRJ.7.000939.
(38) Suebka, S.; Nguyen, P.-D.; Gin, A.; Su, J. How Fast It Can Stick: Visualizing Flow Delivery to Microtoroid Biosensors. *ACS Sens.* **2021**, *6* (7), 2700–2708. https://doi.org/10.1021/acssensors.1c00748.

(39) Li, C.; Lohrey, T.; Nguyen, P.-D.; Min, Z.; Tang, Y.; Ge, C.; Sercel, Z. P.; McLeod, E.; Stoltz, B. M.; Su, J. Part-per-Trillion Trace Selective Gas Detection Using Frequency Locked Whispering-Gallery Mode Microtoroids. *ACS Appl. Mater. Interfaces* **2022**, *14* (37), 42430–42440. https://doi.org/10.1021/acsami.2c11494.
(40) Droulia, M.; Anastasaki, A.; Rokotas, A.; Pitsikalis, M.; Paraskevopoulou, P. Statistical Copolymers of Methyl Methacrylate and 2-Methacryloyloxyethyl Ferrocenecarboxylate: Monomer Reactivity Ratios, Thermal and Electrochemical Properties. *Journal of Polymer Science Part A: Polymer Chemistry* **2011**, *49* (14), 3080–3089. https://doi.org/10.1002/pola.24745.
(41) Kim, B. Y.; Ratcliff, E. L.; Armstrong, Neal. R.; Kowalewski, T.; Pyun, J. Ferrocene Functional Polymer Brushes on Indium Tin Oxide via Surface-Initiated Atom Transfer Radical Polymerization. *Langmuir* **2010**, *26* (3), 2083–2092. https://doi.org/10.1021/la902590u.
(42) Swenson, H.; Stadie, N. P. Langmuir's Theory of Adsorption: A Centennial Review. *Langmuir* **2019**, *35* (16), 5409–5426. https://doi.org/10.1021/acs.langmuir.9b00154.
(43) N'Diaye, M.; Pascaretti-Grizon, F.; Massin, P.; Baslé, M. F.; Chappard, D. Water Absorption of Poly(Methyl Methacrylate) Measured by Vertical Interference Microscopy. *Langmuir* **2012**, *28* (31), 11609–11614. https://doi.org/10.1021/la302260a.